Geophys. J. R. astr. Soc. (1983) 75, 1–21

Stress corrosion and acoustic emission during tensile crack propagation in Whin Sill dolerite and other basic rocks

P. G. Meredith and B. K. Atkinson *Geology Department, Imperial College of Science and Technology, Prince Consort Road, London SW7 2BP*

Received 1983 January 26; in original form 1982 January 25

Summary. Double torsion tests in ambient air and liquid water have been used to establish critical stress intensity factors (K_{Ic}) and stress intensity factor (K_I)–crack velocity (v) diagrams for propagation of single tensile cracks in Whin Sill dolerite and Ralston Intrusive. K_{Ic} for Whin Sill dolerite was 3.28 MN $m^{-3/2}$ and for Ralston Intrusive was 2.58 MN $m^{-3/2}$. No stress corrosion limit was encountered.

Acoustic response was monitored during experiments on Whin Sill dolerite which spanned a velocity range from 5×10^{-4} to 5×10^{-9} m s^{-1}. The rate of acoustic emission was an indirect measure of crack velocity. The slopes of K_I–v diagrams and K_I–acoustic emission rate diagrams had similar slopes of *c.* 30 in double logarithmic coordinate frames. Slopes of the K_I–v curves for Ralston Intrusive fell from 43.4 in air to 23.3 in water, during tests which spanned a crack velocity range from 5×10^{-4} to 10^{-8} m s^{-1}.

The activation enthalpy for dolerite between 20° and 75°C was determined by two complementary methods to be 30.4 ± 1.9 and 33–46 kJ mol^{-1}.

Amplitude distributions of acoustic emission events depend strongly on K_I and the 'humidity' at the crack tip. As K_{Ic} is approached, b-values for dolerite in air decrease from 1.8 to 1.25, and for dolerite in water a decrease occurs in b-value from 3.5 to 1.25. At K_I greater than 0.8 K_{Ic} the b-values for tests in water and in air are virtually identical.

A discussion is given of these results in terms of their implications for earthquake mechanics.

1 Introduction

Subcritical tensile crack growth due to stress corrosion is now regarded as an important mechanism of rock fracture (Atkinson 1982, 1983). It has been proposed that stress corrosion may be of crucial importance in time-dependent earthquake phenomena (Das & Scholz 1981) and in the physico-chemical changes that occur in rock properties throughout earthquake preparation zones (Crampin, Evans & Atkinson 1984). A large proportion of the Earth's seismogenic regions lie in basic rocks (e.g. mid-oceanic fracture zones) so it is of considerable importance that the fracture properties of this class of rocks are well known.

We present here some new experimental results on subcritical, stress corrosion crack growth in Whin Sill dolerite and Ralston Intrusive and we compare these data with results obtained by ourselves and others for various basic rocks. In addition, we have monitored the acoustic response of Whin Sill dolerite during stress corrosion crack growth and these data are also compared with other results. Atkinson & Rawlings (1981) have suggested that acoustic emission characteristics during subcritical, tensile crack growth can be a useful guide to crack velocity, crack tip environment and the approach of a rock to failure.

2 Theoretical considerations

2.1 GENERAL

This study is based on the theoretical framework of fracture mechanics (Irwin 1958) as modified in the light of experimental observations on subcritical cracking in ceramics and glasses (Wiederhorn 1974, 1978) and in rocks (Atkinson 1982, 1983). The most important parameter in this analysis of crack propagation is the stress intensity factor at the crack tip (K_I), which for tensile (mode I) cracks is given by

$$K_I = \sigma_a Y(\pi a)^{1/2} \tag{1}$$

where σ_a is a remote applied stress, Y is a geometrical constant and a is a characteristic crack length. For elliptical, slit-like cracks a is half the crack length. Catastrophic crack propagation occurs at a velocity approaching that of sound in the medium when K_I attains a critical value, K_{Ic}, called the fracture toughness. This parameter is independent of specimen geometry and loading configuration and is thought of as a material constant in the same way as the elastic constants. For further basic information on fracture mechanics see Lawn & Wilshaw (1975).

2.2 SUBCRITICAL CRACK PROPAGATION

There is now a large body of experimental evidence which supports the idea that quasi-static subcritical crack growth involving stress corrosion can occur in rocks at values of K_I often far below that of K_{Ic} (Atkinson 1982). There is some evidence from work on glasses and ceramics (Wiederhorn 1974, 1978) that there exists at about $0.1-0.25 K_{Ic}$ a threshold stress intensity factor, K_0, below which no crack propagation occurs. A threshold has not been positively identified in any study on rocks, but presumably one must exist even if the value of K_0 is rather uncertain (see Atkinson 1983).

Atkinson (1982, 1983) has reviewed some of the theories used to describe subcritical crack growth in materials and concluded that the most useful description at the present time is the Charles equation (Charles 1958) which when recast in terms of fracture mechanics becomes

$$v = v_0 \exp(-H/RT) K_I^n \tag{2}$$

where v is the crack velocity, v_0 and n are constants, H is the activation enthalpy, R is the gas constant and T is the absolute temperature. Equation (2) can be usefully simplified to

$$v = \alpha K_I^n \tag{3}$$

where $\alpha = v_0 \exp(-H/RT)$. The parameter n is known as the subcritical crack growth index.

Fig. 1 shows a schematic $K_I - v$ diagram which uniquely describes the crack propagation behaviour for a given environment. Upon raising K_I above K_0 region 1 behaviour is observed. In this region the crack growth rate is controlled by stress corrosion reactions at the crack tip. At higher values of K_I in region 2 the crack velocity is apparently controlled by the rate

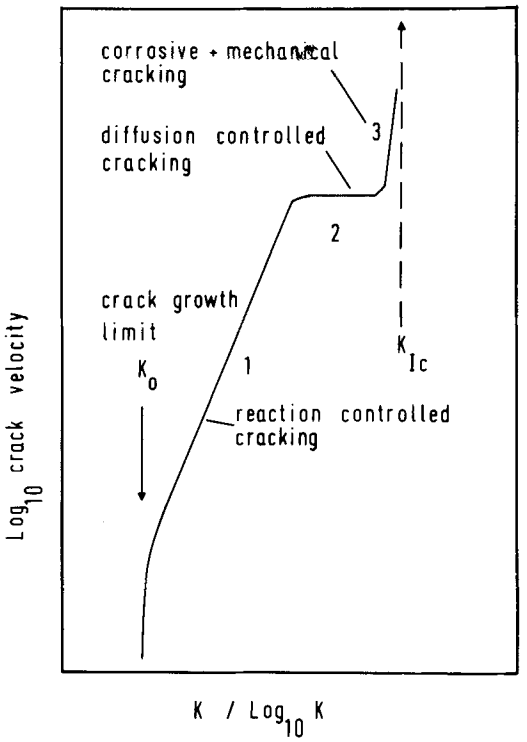

Figure 1. Schematic stress intensity factor/crack velocity diagram for a material undergoing stress corrosion.

of transport of reactive species to the crack tip. As K_I is increased even further, into region 3, the $K_I - v$ curve asymptotically approaches K_{Ic} and failure. In this region mechanical cracking becomes increasingly dominant and the crack velocity is relatively insensitive to environmental conditions.

2.3 THE DOUBLE TORSION TESTING METHOD

Crack propagation was studied by using the double torsion testing method which has been employed extensively for the study of subcritical crack growth in geological materials, both by ourselves (Atkinson 1979b, 1980; Atkinson & Meredith 1981; Atkinson & Rawlings 1981; Meredith & Atkinson 1982) and by other workers (reviewed in Atkinson 1982, 1983). The major advantage of this method is that K_I is independent of crack length over much of the specimen and that a complete $K_I - v$ diagram may be generated from the results of a single load relaxation test.

A schematic drawing of the double torsion specimen is given in Fig. 2. The double torsion plates used in this study measured approximately $12 \times 6 \times 0.4$ cm and each was centrally grooved along the length of its lower surface to a depth of 1/3 of its thickness.

There has been some recent discussion in the literature on the validity of the double torsion testing method (see Swanson 1983 and Atkinson 1983 for summaries). The main problems relate to the dimensions of the specimen with respect to key parameters such as crack length and grain size. Crack length must be kept within the region of the specimen that gives a constant K-calibration. Appropriate guidelines are summarized by Swanson

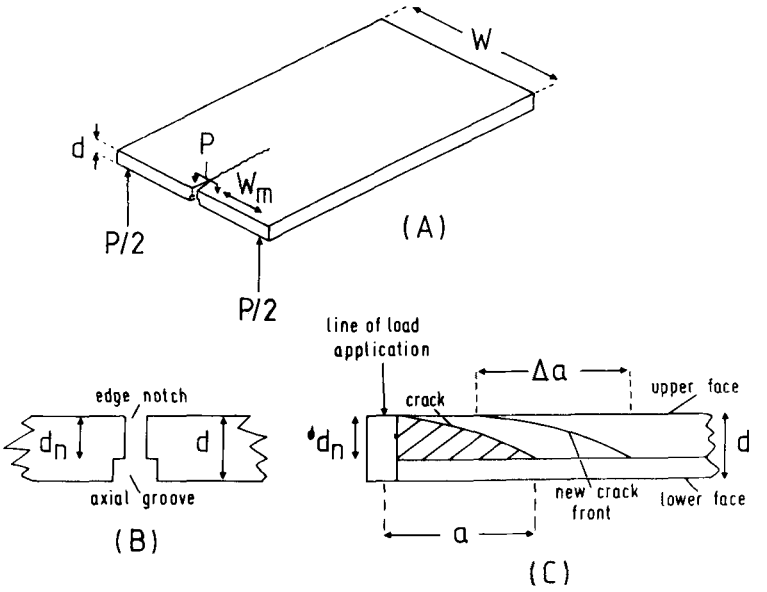

Figure 2. Schematic drawing of a double torsion specimen. (A) General view. (B) Axial cross-section. (C) Longitudinal cross-section.

(1983) and Atkinson (1983). The present double torsion experiments were always arranged so that after precracking the crack length fell in the range 0.25–0.7 of the specimen length. This range has been found by Trantina (1977) in a finite element analysis to give constant K data for our specimen geometry.

Another criticism is that the double torsion method may not be truly representative of tensile (mode I) loading and some mode III (anti-plane shear) loading may occur. Evans (1972) disposed of this criticism at the same time as he originally raised the problem. Moreover, Fuller (1979) notes that in a well set up assembly, opening can be the only mode of fracture in a double torsion specimen, since the loading configuration and the specimen geometry are symmetrical about the crack plane. More recently Cox & Atkinson (1982) have shown that mode III critical stress intensity factors are generally not the same as mode I values for rocks. Because Meredith, Atkinson & Hillman (1981) have shown that there is a rather good correlation between values of fracture toughness measured with the double torsion specimen and those measured with the short rod specimen (an undeniably mode I test method), it follows that double torsion tests must put the crack propagation dominantly into mode I.

Stress intensity factors for the double torsion specimen geometry are given by Williams & Evans (1973) as

$$K_I = P W_m [3(1+\nu)/W d^3 d_n]^{1/2} \tag{4}$$

where P is the applied load, ν is Poisson's ratio, d is the specimen thickness, d_n is the reduced thickness in the plane of the axial groove and the other variables are as shown in Fig. 2. Provided that the initial crack length is in the constant K region then crack velocity may be obtained from the load relaxation data using the equation (Williams & Evans 1973)

$$v = -\phi a_f P_f (1/P^2)(dP/dt) \tag{5}$$

where a_f and P_f are respectively the crack length and load which are measured at the end of

a test and t is the time. ϕ is a geometrical constant which accounts for the curvature of the propagating crack front (Evans 1972; Atkinson 1979b).

2.4 ACTIVATION ENTHALPIES

The activation enthalpy for crack propagation may be obtained by two complementary methods.

(1) A family of $K_I - v$ curves may be constructed from tests conducted at different temperatures, but otherwise in the same environments, using equations (4) and (5). For a change in temperature from T_1 to T_2 at constant crack velocity the activation enthalpy (H) is given by

$$H = [R T_2 T_1/(T_2 - T_1)]\, n \ln(K_{I1}/K_{I2}) \tag{6}$$

where n and H are generally found to be insensitive to temperature changes over restricted ranges of the parameter (Evans 1972; Atkinson 1979b, 1980; Meredith & Atkinson 1982).

(2) Evans (1972) has shown that for the double torsion geometry

$$\dot{y} = A K_I v \tag{7}$$

where $\dot{y}$ is the displacement rate and A is a constant which depends on the specimen and apparatus geometry and the elastic modulus and is obtained from compliance measurements. Substituting for v in equation (7) gives

$$\dot{y} = A v_0 \exp(-H/RT)\, K_I^{n+1}. \tag{8}$$

By analogy with method (1) above, for a change in temperature from T_1 to T_2 at constant displacement rate

$$H = [RT_2 T_1/(T_2 - T_1)]\,(n+1) \ln(K_{I1}/K_{I2}). \tag{9}$$

2.5 ACOUSTIC EMISSION

Acoustic emission is the term used for the transient elastic waves generated in a solid by rapid, usually localized, stress or strain relaxations accompanying such deformation mechanisms as the nucleation or growth of cracks, or the propagation of dislocations. When these elastic waves hit a piezoelectric transducer it is stimulated to give as output a series of wave packets. Each packet is termed an acoustic emission event. The number of wave crests in the wave packet that exceed some instrumentally set threshold is the ring-down count for that event. It is a crude measure of the energy of an acoustic emission event. The events are further characterized by the peak amplitude of the waveform. The relation between the number of acoustic emission events and their peak amplitudes can be studied in amplitude–frequency diagrams. They can shed light on the mechanisms of acoustic emission.

Acoustic emission studies on rock and most other materials are rather qualitative at present, however, and are not sufficiently refined to give detailed quantitative information on deformation mechanisms. The physical details of acoustic emission have only just begun to be probed in a quantitative way for a few metals (see Wadley, Scruby & Shrimpton 1981). The method used requires very unusual specimen geometry (Yobell specimen) that allows both simple mode I loading and yet is sufficiently like an elastic half-space to allow valid application of source and transfer function theories. The specimen reduces the potential source of emissions to just a few grains and grain boundaries. It is not possible at present to produce similar complex shaped specimens for rocks.

3 Test materials

The dolerite used in this study was collected from the Great Whin Sill in Upper Teesdale, Durham, and is similar to that described by Harrison (1968). It is a grey quartz-dolerite with a groundmass grain size that varies from 0.1 to 0.6 mm. A few clino-pyroxene microphenocrysts and ilmenite-magnetite intergrowths may attain lengths of up to *c.* 2 mm.

The Ralston Intrusive is a dark-grey monzonite from the Ralston dyke near Golden, Colorado. It consists of microphenocrysts of glassy feldspar and augite in an aphanitic groundmass (grain size *c.* 10 μm).

Table 1. Modal analyses (in volume per cent) of test materials.

Whin Sill dolerite	Ralston Intrusive	Black gabbro
pl 48, cpx 29, op 8, qz 5, opx 4, others 6	af 36, pl 28, ag 23, op 6, ol 4, others 3	pl 50, cpx 38, op 8, fqe 3, others 1

Key: pl = plagioclase, cpx = clino-pyroxene, opx = ortho-pyroxene, af = alkali feldspar, op = opaques, qz = quartz, ag = augite, ol = olivine, fqe = feldspar/quartz eutectic.

Table 2. Comparison of measured fracture toughness values for basic rocks with those for some other rock types. Grain size data for rocks are also presented.

Rock type	K_{Ic} (MN m$^{-3/2}$)	Grain size (mm)	Testing method	Reference
Whin Sill dolerite	3.28 ± 0.10	0.1–0.6 (2.0)	DT	This study
Ralston Intrusive	2.58 ± 0.06	0.01	DT	This study
Black gabbro	2.88 ± 0.05	0.4–1.0	DT	Atkinson & Rawlings (1981)
Preshal More basalt	2.50 ± 0.14	0.07 (0.1–0.25)	SR	Meredith *et al.* (1981)
Quartz	0.85–1.0	–	DT	Atkinson (1983)
Arkansas novaculite	1.34	0.01	DT	Atkinson (1980)
Mojave quartzite	2.1	0.20	DT	Atkinson (1983)
Solnhofen limestone	0.78–1.01	0.005	DT 3PB	Atkinson (1983)
Westerly granite	1.74	0.75	DT	Atkinson & Rawlings (1981)

Key: DT = double torsion, SR = short rod, 3PB = three point bend. Grain size figures in brackets refer to phenocrysts.

Modal analyses of both rocks, from Harrison (1968) and van Horn (1976) respectively, are given in Table 1, together with data for the Black gabbro tested by Atkinson & Rawlings (1981) for comparison. This gabbro has a grain size which varies from 0.4 to 1.0 mm.

The Preshal More basalt, for which a K_{Ic} figure is quoted in Table 2, is an olivine-basalt with a maximum groundmass grain size of *c.* 0.07 mm and microphenocrysts of plagioclase, olivine and oxides which can attain a size of 0.4 mm, but generally are in the range from 0.1 to 0.25 mm.

4 Experimental details

All experiments were performed using an Instron Corporation universal testing machine to deform specimens inside an environmental chamber. Both the environmental chamber and the loading arrangements have been described in detail by Atkinson (1979b) and are not repeated here.

4.1 FRACTURE TOUGHNESS TESTS

These were performed in air of ambient humidity on specimens which had previously been pre-cracked at a slow loading rate following procedures described by Atkinson (1979a). A rapid cross-head velocity of 2.5 cm min^{-1} was then used to propagate the crack to catastrophic failure. Meredith & Atkinson (1982) have shown that this cross-head velocity is sufficiently fast to eliminate any influence on K_{Ic} of water vapour in the environment. The peak load sustained under fast loading was used to calculate K_{Ic} from equation (4).

4.2 LOAD RELAXATION TESTS

Load relaxation tests were performed in air of 20 per cent RH and in liquid water at 20 and 75°C. Pre-cracked specimens were loaded at a rapid cross-head velocity to a load close to that for catastrophic crack propagation. At this point the cross-head was stopped and the load on the specimen was allowed to decay as a result of slow, stable crack extension.

In the majority of tests the load/time data were recorded on a strip chart recorder. The data from at least one test at each set of environmental conditions were recorded on a fast capture digital storage oscilloscope. This allowed the load/time trace to be expanded and enabled data to be obtained at higher crack velocities than would otherwise have been possible.

$K_I - v$ digrams were constructed from the load relaxation data using equations (4) and (5). An estimate of H was calculated from the separation of isotherms using equation (6). The reader is referred to Meredith & Atkinson (1982) for a discussion of the experimental precautions required to ensure the high quality of load relaxation data.

4.3 CONSTANT DISPLACEMENT RATE TESTS

In these experiments the specimens were deformed at a constant, low displacement rate of 0.005 cm min^{-1} until the crack propagated to failure at a constant stress intensity factor (see Evans 1972 for further details). A series of tests were performed at different temperatures and H was calculated from the values of K_I at failure using equation (9). This method of calculating H is not subject to the sources of error that influence the calculation of H from load relaxation data.

4.4 ACOUSTIC EMISSION MONITORING

Acoustic emission (AE) was monitored during each of the room temperature relaxation tests on Whin Sill dolerite using standard Dunegan/Endevco 3000 series equipment. This enabled us to monitor simultaneously AE event rates, ring-down count rates and amplitude/frequency distributions. In all experiments a stainless steel waveguide consisting of a 15 cm length of 0.64 cm diameter rod with conical terminations was used to conduct the AE signals from the specimen to an AE transducer located outside the environmental chamber. The waveguide was bonded to both the transducer and the specimen with epoxy resin to ensure

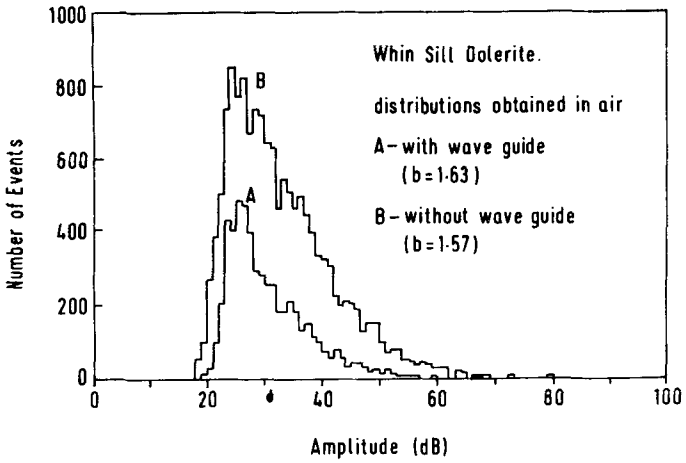

Figure 3. Comparison of acoustic response of Whin Sill dolerite with and without a waveguide. Number of AE events is plotted against event amplitude in dB.

a good acoustic contact. The transducer had a high response band between 100 and 500 kHz. AE signals with a frequency below 100 kHz and above 350 kHz were filtered out.

Amplitude distributions were obtained by sorting events into 100 bins or receptacles each 1 dB wide. The amplitude–frequency data are represented by a power law of the form (Pollock 1973)

$$n(V) = (V/V_0)^{-b}. \tag{10}$$

where $n(V)$ is the fraction of the emission population whose peak amplitude exceeds V, V_0 is the lowest detectable amplitude and b is the exponent which characterizes the amplitude distribution. Equation (10) has been used successfully by Atkinson & Rawlings (1981) to describe their experimental data for stress corrosion cracking in granite and gabbro. An important feature of this equation is that the b-value does not change if the amplitudes of all events are reduced by the same factor. Thus, attenuation due to the AE sources being remote from the AE transducer should not influence measurements of b.

The acoustic response of Whin Sill dolerite both with and without a waveguide was measured using the same AE transducer. Double torsion plates were loaded at a cross-head velocity of 0.05 cm min^{-1} until catastrophic failure occurred. The resulting amplitude distributions are shown in Fig. 3. Although the waveguide causes some loss of sensitivity, the form of the amplitude distributions (b-values) are virtually unchanged.

5 Fracture mechanics results

The K_{Ic} values obtained for Whin Sill dolerite, Ralston Intrusive and other basic rock types are given in Table 2. Whin Sill dolerite has the highest K_{Ic} of any rock yet tested in our laboratory.

Results of load relaxation experiments on Whin Sill dolerite in ambient air at 20°C and in liquid water at 20 and 75°C are shown in Fig. 4. Similar results for Ralston Intrusive in ambient air and liquid water at 20°C are shown in Fig. 5. The solid lines are fitted by regression analysis of the data points, and their slopes (the subcritical crack growth index, n) are given in Table 3 in comparison with values for other rocks of basic composition (see also Table 4).

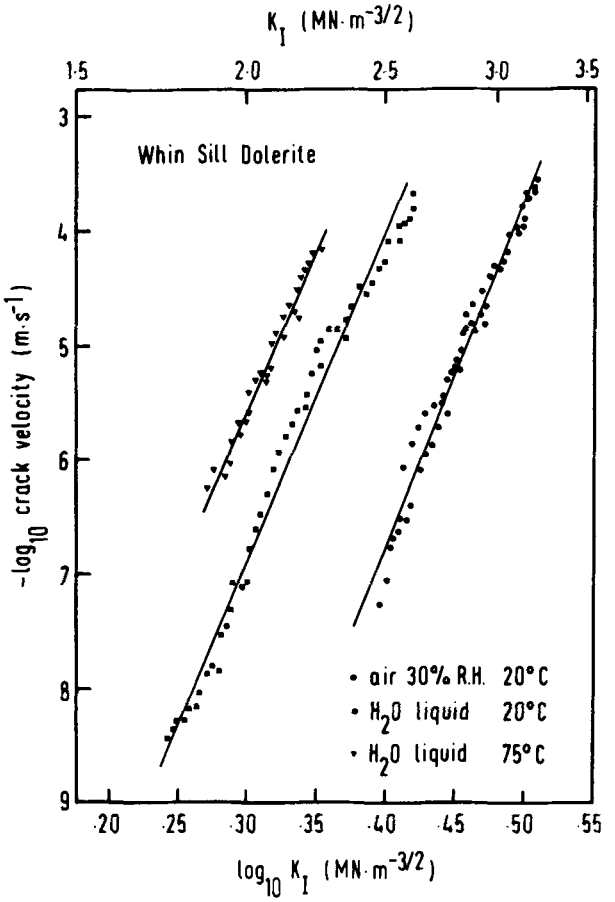

Figure 4. Stress intensity factor/crack velocity diagram for Whin Sill dolerite cracked in ambient air at 20°C and in liquid water at 20 and 75°C. Data are from load relaxation experiments.

The activation enthalpy for crack propagation in Whin Sill dolerite calculated using the data of Fig. 4 and equation (6) was 33 to 46 kJ mol^{-1}. Using constant displacement rate data and equation (9), the activation enthalpy was 30.4 ± 1.9 kJ mol^{-1}.

Note that all the data of Figs 4 and 5 pertain to region 1 of the schematic $K_I - v$ diagram shown in Fig. 1. We reach this conclusion because if the data pertained to region 2 of Fig. 1 the slope of the $K_I - v$ curve should be much shallower, more like a plateau. If the data pertained to region 3 of Fig. 1 the $K_I - v$ curve should be much steeper than is actually observed and instead of the strong influence of chemical environment on $K_I - v$ curves noted in these experiments the data should be almost insensitive to changes in chemical environment.

6 Acoustic emission results

6.1 AE EVENT AND RING-DOWN COUNT RATES

As stated earlier, both AE event rates and ring-down count rates were measured simultaneously with crack velocities during load relaxation tests on the dolerite. These data are

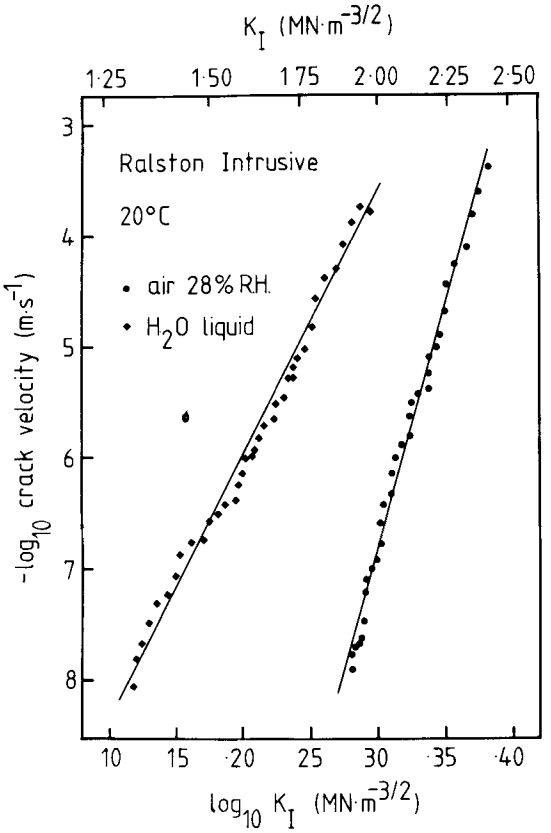

Figure 5. Stress intensity factor/crack velocity diagram for Ralston Intrusive cracked in ambient air and in liquid water at 20°C. Data are from load relaxation experiments.

Table 3. Compilation of stress corrosion indices for basic rocks.

Rock type	Conditions	Stress corrosion index (n)	Reference
Whin Sill dolerite	Air, 30 per cent RH, 20°C	31.2	This study
	Water, 20°C	29.0	This study
	Water, 75°C	28.4	This study
Ralston Intrusive	Air, 28 per cent RH, 20°C	43.4	This study
	Water, 20°C	23.3	This study
Black gabbro	Air, 30 per cent RH, 20°C	32.1	Atkinson & Rawlings (1981)
	Water, 20°C, region 1	28.6	Atkinson & Rawlings (1981)
	Water, 20°C, region 3	36.1	Atkinson & Rawlings (1981)
Murata basalt	Air, 20°C	22	Sano & Ogino (1980)
Kinosaki basalt	Air, 30°C	~34	Waza, Kurita & Mizutani (1980)
	Water, 25°C	~33	Waza *et al.* (1980)

shown as a function of stress intensity factor in Figs 6 and 7, which should be compared with Fig. 4.

The form of the curves in Figs 4, 6 and 7 is very similar and we can, therefore, follow Atkinson & Rawlings (1981) in using similar equations to (3) to describe the acoustic

Table 4. Values of n, n_E and n_R for Whin Sill dolerite in different environments.

	Air, 30 per cent RH, 20°C	Water, 20°C	Water, 75°C
n	31.2 (0.990)	29.0 (0.992)	28.4 (0.995)
n_E	31.1 (0.984)	29.1 (0.977)	
n_R	32.9 (0.981)	29.9 (0.973)	

Figures in brackets are correlation coefficients.

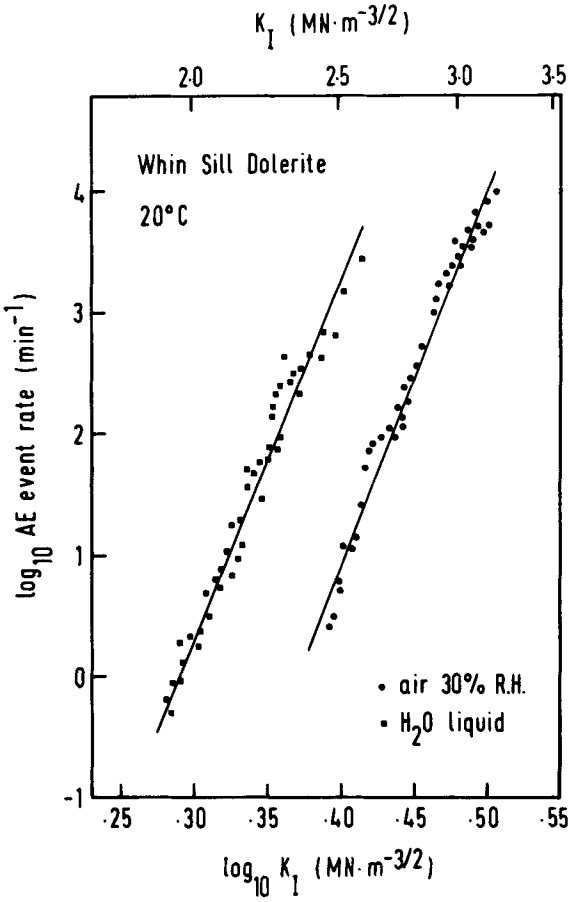

Figure 6. Plot of log AE event rate against log stress intensity factor for Whin Sill dolerire cracked in ambient air and water at 20°C.

emission – K_I data. Making this assumption, the AE event rate (dN_E/dt) is given by

$$dN_E/dt = \beta K_I^{n_E} \tag{11}$$

and ring-down count rate (dN_R/dt) is given by

$$dN_R/dt = \gamma K_I^{n_R} \tag{12}$$

where β and n_E and γ and n_R are constants comparable to α and n in equation (3). Because of the similar form of the equations used to describe emission rates and crack velocities as a

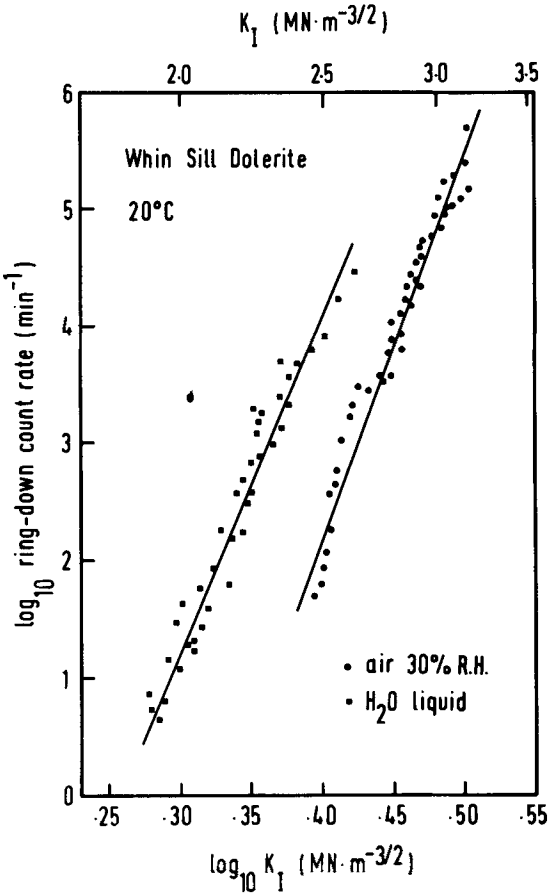

Figure 7. Plot of log ring-down count rate against log stress intensity factor for Whin Sill dolerite cracked in ambient air and water at 20°C.

function of K_I, then it is reasonable to compare the slopes of the curves (i.e. n, n_E and n_R). This comparison is shown in Table 4.

It should be noted that significant acoustic emission rates were measured even at the lowest crack velocities encountered, and that because of the close similarity in the values of the three exponents for a given environment, the acoustic emission rates can be used as an indirect measure of crack velocity. This confirms and extends the findings of Atkinson & Rawlings (1981). Note also, however, that the stability of the apparatus/specimen assembly limits the lowest crack velocities and AE emission rates that can be studied.

6.2 AMPLITUDE DISTRIBUTIONS

Plots of amplitude distributions for tests on dolerite in air and water are shown in Figs 8 and 9, respectively. The stress intensity factor range and b-value for each curve are given on the diagrams. The b-values are generally higher for 'wet' tests than for 'dry' tests at a given level of stress, but decrease with increasing K_I for both data sets. Physically this means that at high values of K_I the deformation process is characterized by a high proportion of large events so that b is relatively low; and at lower values of K_I there is a higher proportion of small events so that b is relatively high (Pollock 1973; Atkinson & Rawlings 1981).

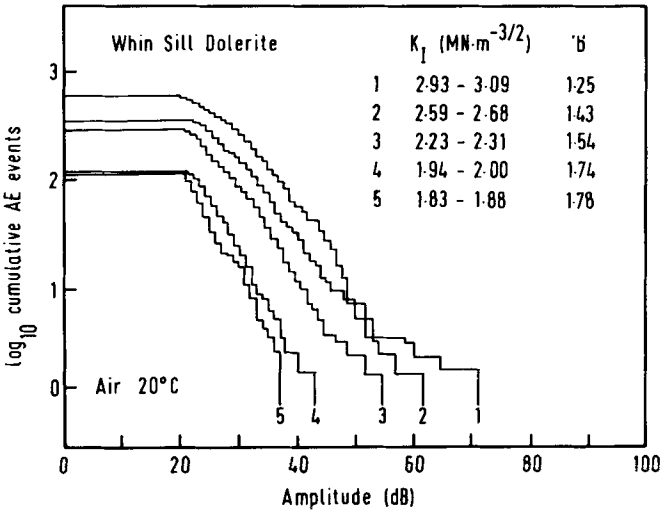

Figure 8. Typical amplitude distributions for Whin Sill dolerite cracked in ambient air at 20°C. Stress intensity factor ranges and *b*-values are shown on the diagram.

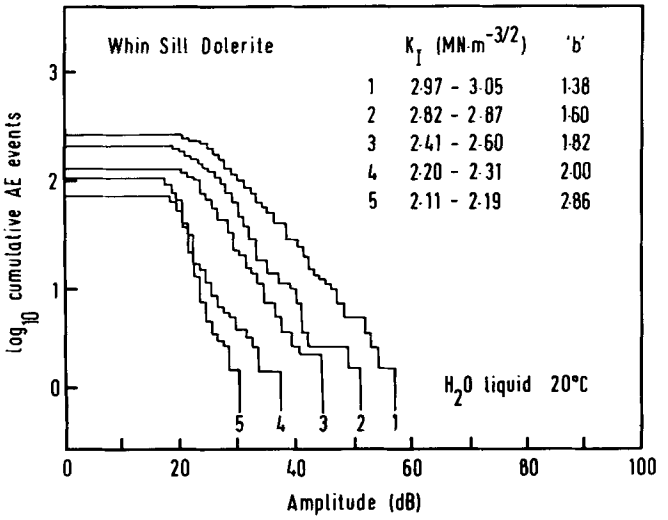

Figure 9. Typical amplitude distributions for Whin Sill dolerite cracked in liquid water at 20°C. Stress intensity factor ranges and *b*-values are shown on the diagram.

The *b*-values from Figs 8 and 9 are plotted against K_I and normalized K_I (i.e. K_I/K_{Ic}) in Fig. 10. This figure shows very clearly the behaviour noted above that *b*-values for tests in water are generally higher than those in air, but trend towards the same value at high values of K_I, and also exhibit a more marked dependence on K_I. Fig. 11 is a synoptic diagram showing *b*-value data for three crustal rocks as a function of 'humidity' at the crack tip and K_I/K_{Ic}. It is of particular interest to note the great similarity in the trends of the data for granite, gabbro and dolerite.

These observations are consistent with the idea that at low K_I, and hence low crack velocity, different crack propagation mechanisms operate in wet and dry dolerite, gabbro and granite, but that at high K_I, and high crack velocity, the mechanism of crack growth is relatively insensitive to environmental conditions.

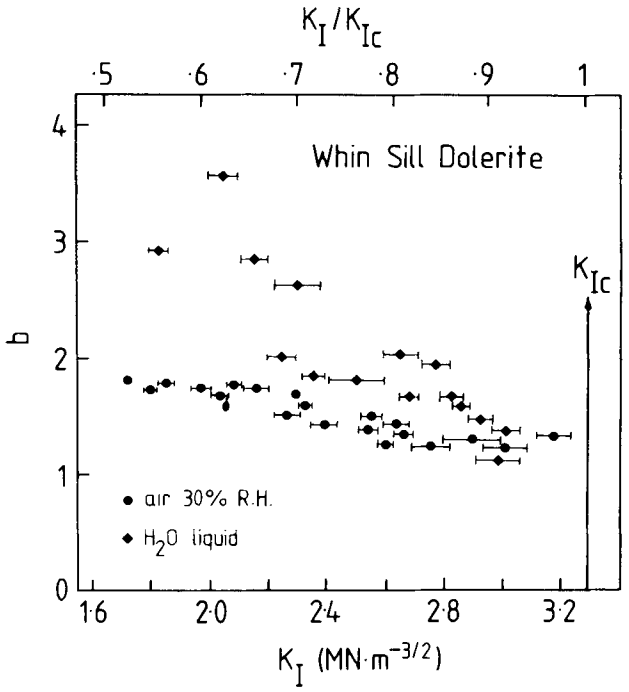

Figure 10. Amplitude distribution parameter (b) against stress intensity factor and normalized stress intensity factor for Whin Sill dolerite. Horizontal bars denote stress intensity range. Circles denote tests in air of 30 per cent RH. Diamonds denote tests in liquid water.

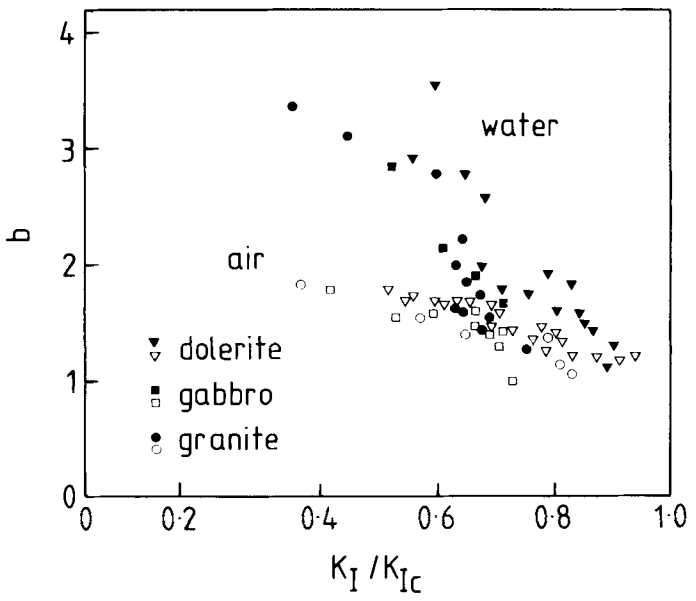

Figure 11. Synoptic diagram of b-value data as function of 'humidity' at crack tip and normalized K_I (i.e. K_I/K_{Ic}) for dolerite (this study), gabbro and granite (Atkinson & Rawlings 1981). Closed symbols: double torsion tests in liquid water. Open symbols: double torsion tests in air of 30 per cent RH.

6.3 AVERAGE AMPLITUDE DATA

Pollock (1980) has stated that the introduction of average amplitude processing is one of the most successful approaches to acoustic emission analysis. Cumulative ring-down count (ΣN_R) is a good approximation to the sum of the amplitudes of all AE events, i.e. the product of the cumulative number of events (ΣN_E) and average amplitude of events (Dilipkumar, Gudimetla & Wood 1979). If ΣN_R is plotted against ΣN_E, then the slope of the resultant curve is a measure of average amplitude. An average amplitude parameter may be obtained, therefore, by monitoring ΣN_R and ΣN_E during a test (Pollock 1974; Dilipkumar *et al.* 1979).

Any change in the amplitude distribution during a test will be reflected in a change in the relationship between ΣN_E and ΣN_R. One significant experimental advantage of this method is that it eliminates the need to obtain actual amplitude distribution histograms.

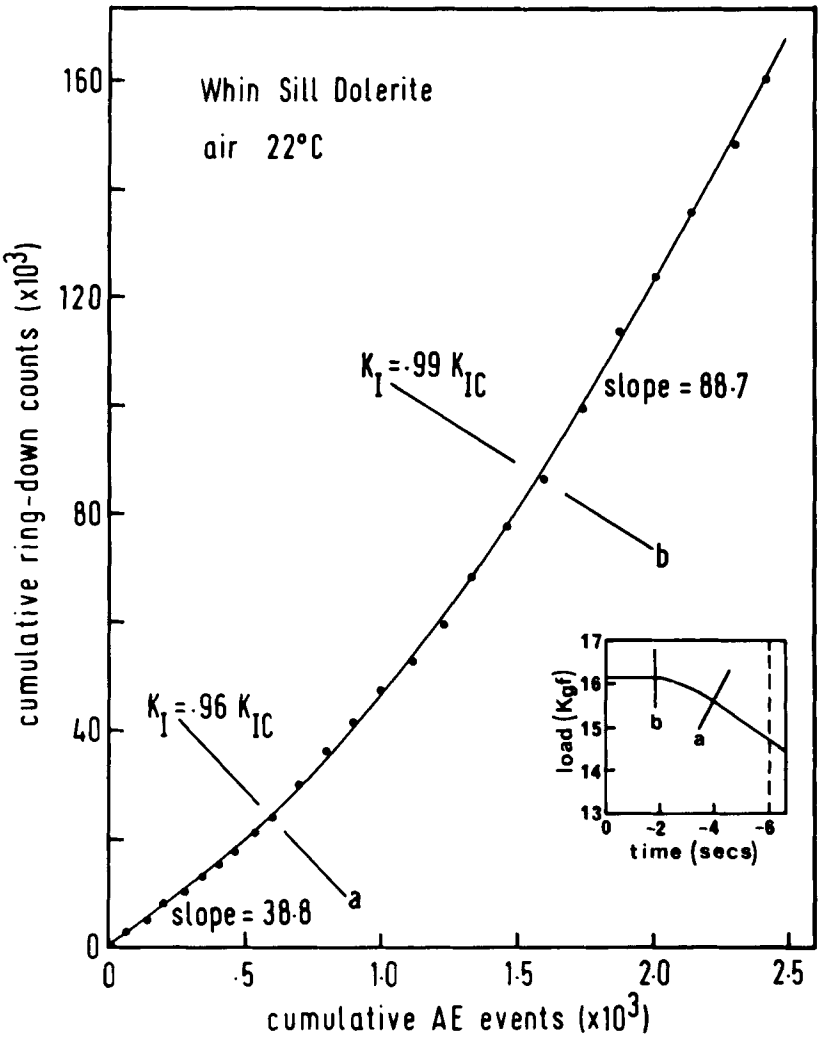

Figure 12. Plot of cumulative AE events against cumulative ring-down counts for Whin Sill dolerite tested in ambient air. Inset shows the load/time trace for the same segment of the test.

We performed tests on double torsion plates of Whin Sill dolerite in ambient air to obtain average amplitude data at high values of K_I, close to K_{Ic}. Specimens were deformed at a moderate cross-head speed (0.1 cm min^{-1}) until the crack propagated at constant velocity to failure. ΣN_E and ΣN_R data were captured simultaneously using a digital storage oscilloscope.

The results of a typical tests are shown in Fig. 12, with the load/time trace inset. Only data for the high K_I part of the test are shown. These emissions correspond to crack velocities which are unattainable during normal load relaxation tests. Note the sharp change in slope (>2) as K_I is increased from 0.96 K_{Ic} to 0.99 K_{Ic}, signifying a change to a much higher proportion of large amplitude events. This significant change in average amplitude at a high proportion of K_{Ic} may correspond to a change from region 1 to region 3 behaviour as catastrophic failure is approached.

7 Discussion

In discussing these experimental results we will first address the fracture mechanics data and then the findings of acoustic emission monitoring.

Compared to other crustal rocks, the values of K_{Ic} for basic rock types are high (Atkinson 1982, 1983). This means that a greater energy is required to propagate fast fractures in basic rocks than in more acidic crustal rocks.

There is a general tendency for the K_{Ic} values of coarser-grained basic rocks to be greater than those for fine-grained ones. This is a commonly quoted effect for ceramics and is attributed to a change in the balance of fracture mechanism from predominantly intergrannular fracture at very small grain size to predominantly transgranular fracture at large grain size (e.g. Davidge 1974). A similar pattern of behaviour has also been noted for quartz rocks (Atkinson 1983). A physical explanation of why fracture toughness (or its equivalent, fracture energy) for large grained materials is generally greater than that for fine grained materials is that the concentration of grain boundary defects is greater for fine grain sizes. Although there are many conflicting and complicating factors, the fracture toughness of grain boundaries (impurities, porosity, second phase particles and imperfect bonding) tend to weaken them.

The stress corrosion indices, n, for the coarse-grained basic rocks (Whin Sill dolerite and Black gabbro) are very similar (Table 3) despite differences in their mineralogy and grain size. Rather more variation is found in n-values for the basaltic rocks, but this may be attributable to the variation in porosity between the test materials and differences in experimental technique. For the tests performed in our laboratory with the same techniques, the variation in n for all basic rock types cracked in liquid water at 20°C is from 20 to 29. From these figures we can infer that there will be a quite pronounced influence of deformation rate and time on strength. This is because the n values observed indicate that there is a quite large range of K_I values that can sustain subcritical cracking. The larger the value of n the smaller is the range of K_I values for which significant rates of subcritical cracking can occur and the smaller is the range of potential time and rate dependence of strength. Some crustal rocks have n values of 50–100 (see Atkinson 1983).

We infer from our scanning electron fractography of dolerite and gabbro that the proportion of grains undergoing transgranular fracture decreases as crack velocity decreases so that intergranular fracture becomes more important. This is shown in Figs 13–16. Figs 13 and 14 show portions of crack surfaces formed at high crack velocities close to those associated with K_{Ic}. They show a large component of transgranular fracturing, although some intergranular fracturing also occurs. At low crack velocities of *c.* 10^{-7} m s^{-1} there is much more crack branching and wandering around grain boundaries and intergranular cracking is more impor-

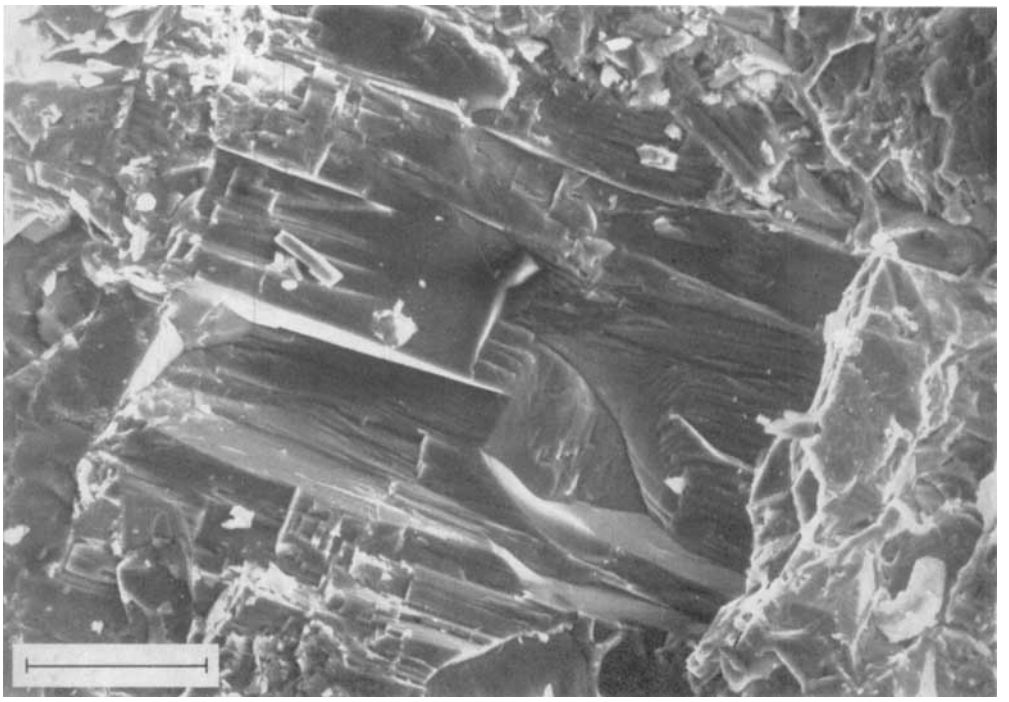

Figure 13. Scanning electron micrograph of fracture surface of Whin Sill dolerite double torsion specimen. Surface was formed at high crack velocity ($> 10^1$ m s^{-1}) during fracture toughness test conducted in air at 20°C. Note the dominance of transgranular fracture cleavage steps and hackle marks. Scale bar $= 75$ μm.

[*facing page* 16]

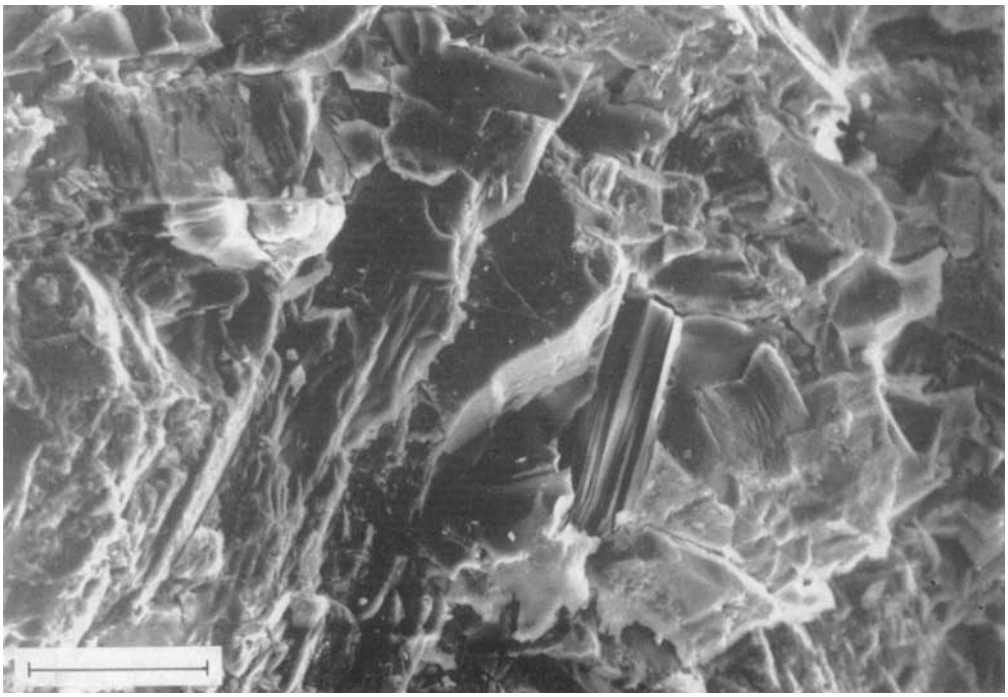

Figure 14. Scanning electron micrograph of fracture surface of Whin Sill dolerite double torsion specimen. Surface was formed under the same conditions as the surface shown in Fig 13. Note the dominance of transgranular fracture, cleavage steps and hackle marks, although intergranular fractures are present. Scale bar = 75 μm.

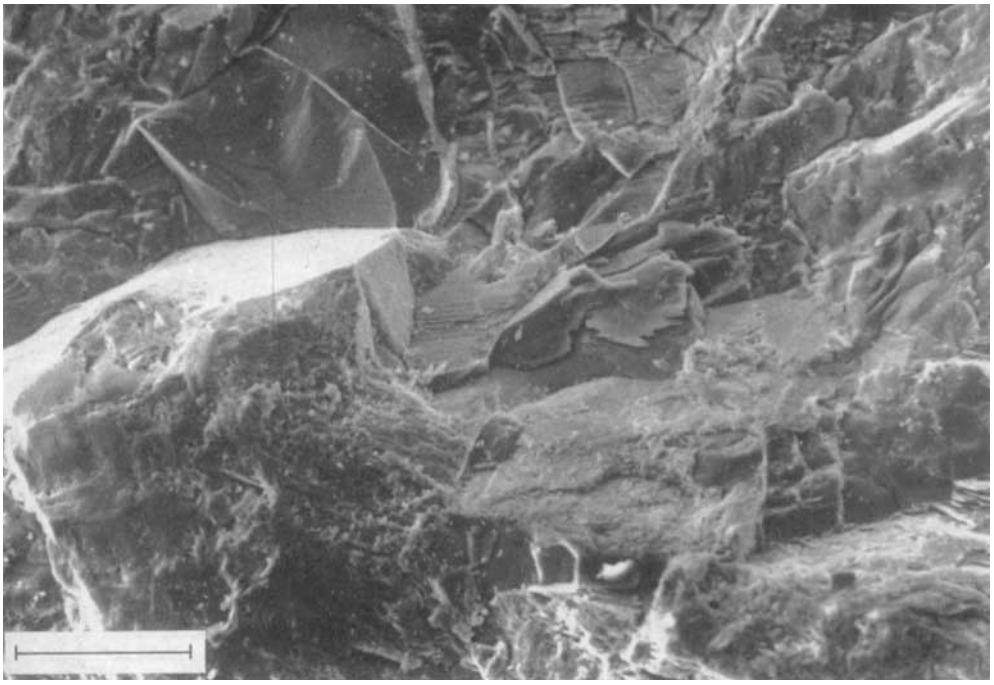

Figure 15. Scanning electron micrograph of fracture surface of Whin Sill dolerite double torsion specimen. Surface was formed at low crack velocity of $c.\ 10^{-7}$ m s^{-1} during load relaxation test conducted in liquid water at 75°C. Note the importance of intergranular fracture, even though transgranular fracture is still evident. Scale bar = 100 μm.

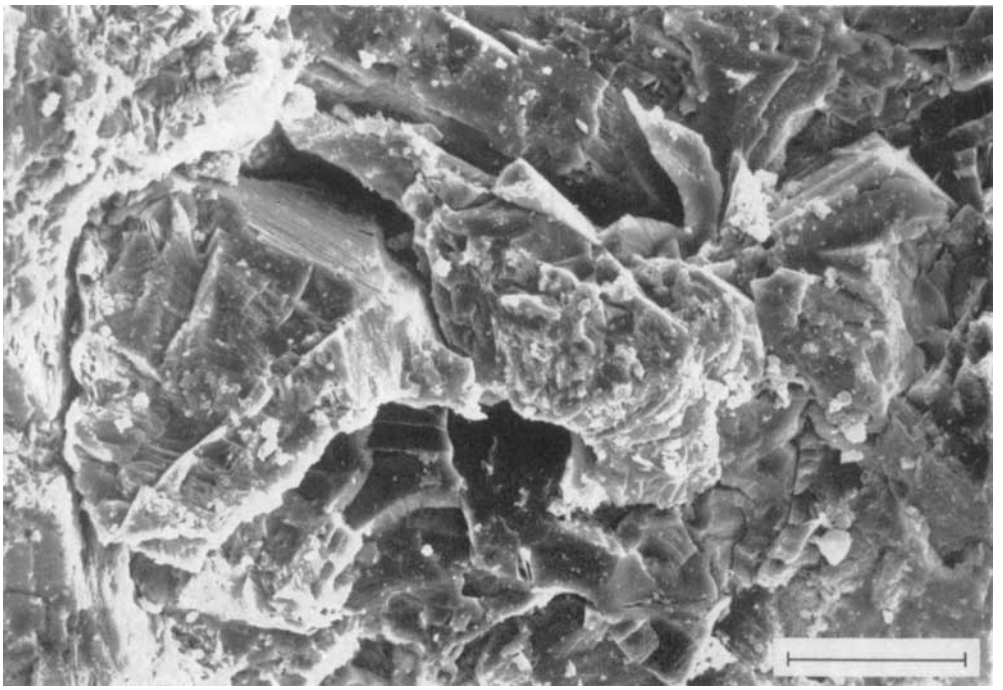

Figure 16. Scanning electron micrograph of fracture surface of Whin Sill dolerite double torsion specimen. Surface was formed at low crack velocity of *c.* 10^{-7} m s^{-1} during load relaxation test conducted in liquid water at 20°C. Note the importance of grain boundary microcracks and the loosening of grains in the macrocrack path, even though transgranular fracture is still evident. Scale bar = 42 μm.

tant than transgranular fracturing (Figs 15 and 16). Similar behaviour has been noted for Westerly granite (Swanson 1980; Atkinson & Rawlings 1981). It can be explained because at low crack velocities (low K_I) the grain boundaries, which are the main access routes for moisture, will stress corrode even before many more highly stressed transgranular cracks.

Das & Scholz (1981) have shown that for their analysis of time-dependent earthquake rupture controlled by stress corrosion crack growth the stress corrosion limit is a key parameter. In our tests on Whin Sill dolerite and Ralston Intrusive in liquid water at 20°C a stress corrosion limit was not encountered even at crack velocities as slow as 10^{-8}–10^{-9} m s^{-1}. This corresponds to stress intensity factors of $0.54\,K_{Ic}$ and $0.48\,K_{Ic}$, respectively. Based upon the data of Wilkins (1980) we suggest that a stress corrosion limit may not be encountered in these rocks until crack velocities are reached that are at least as slow as 10^{-11}–10^{-12} m s^{-1}.

The importance of this suggestion lies in the possibility that subcritical growth of tensile cracks in rocks may be possible at rather low fractions of the critical stress intensity factor. Although at these initially low stress intensity factors the rate of crack growth would be small, on a geological time-scale the cumulative effects of sustained slow cracking could be significant. It should be borne in mind that because crack velocity is a function of K_I, which is itself a function of remote applied stress and crack length, the rate of crack growth will accelerate with the passage of time. An average crack growth rate of 10^{-9} m s^{-1} will give a crack extension of nearly 32 cm in 10 years, while during the same period of time even a crack velocity of 10^{-11} m s^{-1} will give more than 3 mm of crack extension.

Subcritically growing cracks subjected to low stress intensity factors will spend most of their time at the low velocity end of their $K_I - v$ curve before they accelerate to failure. It can easily be shown (Atkinson 1980) that because of this in long-term geophysical processes (involving low stress or slow strain rate) the fast crack velocity data make virtually no difference to predictions of time- and rate-dependent behaviour calculated from $K_I - v$ curves. Thus, although our data pertain only to region 1 of the schematic $K_I - v$ curve (regions 2 and 3 were not encountered) this does not affect their utility in geophysical applications. It is of course also possible that regions 2 and 3 may be of extremely limited extent in our test rocks.

Crampin *et al.* (1984) have proposed a model to explain shallow earthquake precursors that has as its core the hypothesis that when tectonic stress builds up in an earthquake preparation zone subcritical cracking can occur throughout the huge volume of such a region. This low stress dilatancy could give rise to the range of earthquake precursors observed in the field. As it should occur throughout very large volumes of the Earth it could explain the observation of precursors at great distances from the eventual earthquake source region. The present data on basic rocks are consistent with these ideas.

Even a small temperature rise of 55°C is sufficient to increase the rate of crack propagation in dolerite at constant K_I by over an order of magnitude. It is of considerable geophysical interest, therefore, to know how crack propagation is influenced by temperature and pressure increases concomitant with increasing depth in the Earth's crust. The considerable experimental difficulties involved in such a study have so far precluded any direct answer to this problem. The evidence from this study and other recent ones (Atkinson 1979b, 1980; Meredith & Atkinson 1982), however, suggests that stress corrosion growth of cracks in crustal rocks may be accelerated significantly by raising the temperature to those prevailing at the depths of shallow earthquake focal zones. For example, neglecting the unknown influence of pressure and assuming that the $K_I - v$ dependence found at low temperatures also holds at high temperatures then we can calculate crudely the influence on crack velocity in dolerite of temperature changes using equation (2). For a constant K_I, crack velocity in Whin Sill dolerite may increase by 2–3 orders of magnitude as

temperature is raised from 20 to 300°C. This higher temperature would be reached at depths of less than 5 km for distances up to 500 km from oceanic ridge crests, based upon the thermal models for the North Pacific of Parsons & Sclater (1977). But as Atkinson (1983) is at pains to point out, the validity of such extrapolations depends critically on the details of the micromechanism and chemistry of subcritical crack growth.

We noted earlier that detailed studies of acoustic emission source characterization in rocks and most other materials are in their infancy at present, although the quantitative work of Wadley *et al.* (1981) on metals is notably sophisticated. We can, however, make some useful progress in analysing AE source characteristics.

There are potentially four main sources of acoustic emission in these experiments. They are: (1) increments in the primary crack, (2) subsidiary microcracking in the process zone around the main crack tip, (3) dislocation motion and (4) twinning. Sources (3) and (4) can probably be neglected for experiments near room temperature as the minerals in the basic rocks tested show virtually no intracrystalline plastic deformation at these temperatures under the likely crack tip stresses. For Whin Sill dolerite, therefore, this leaves AE sources (1) and (2) to consider.

Acoustic emission from the primary crack is likely to depend on the crack growth rate (Evans, Linzer & Russell 1974; Atkinson & Rawlings 1981) and when the background emission rate is exceeded it is found that (Evans *et al.* 1974)

$$dN/da \propto \ln K_I \tag{13}$$

where dN/da is an event or ring-down count rate with increment in crack length. From an analysis of acoustic emission from subsidiary cracks forming at the perimeter of the process zone around a macrocrack tip in ceramics Evans *et al.* (1974) find that in this case

$$dN/da \propto qK_I^2 \tag{14}$$

where q is the density of microcrack sources. The dependence of microcrack formation stress on time and the statistical nature of grain size and stress at the process zone perimeter were neglected in the derivation of equation (14), but these terms are unlikely to alter the strong K_I^2 dependence of dN/da. Subsidiary microcracking may be a more important contributor to acoustic emission than macrocrack extension if there is a high density of microcrack sources in the process zone.

If source (2) is the predominant source of acoustic emission then we would expect that the rate of emission with increment in crack length would vary with K_I^2 (Evans *et al.* 1974). This is not observed, but instead it is found that the exponents n, n_E and n_R are approximately the same which indicates that rates of acoustic emission with crack increment have a much weaker dependence on K_I and that the majority of acoustic emissions must be due to macrocrack extension (Atkinson & Rawlings 1981). This probably arises because the process zone is likely to be small under the conditions of the present experiments. In another crystalline polyphase rock, Westerly granite, Swanson (1980) was able to locate the sources of acoustic emission. At crack velocities below 10^{-5} m s^{-1} the vast majority of events were associated with the macrocrack tip. AE events associated with microcracking in the process zone ahead of the macrocrack tip were not observed at these velocities.

Evans & Linzer (1973) have noted that AE during subcritical cracking of porcelain in water at 20°C can also be accounted for mainly by macrocrack extension. AE from Lucalox alumina under similar deformation conditions, however, seems to be dominated by microcracking in the process zone (Evans *et al.* 1974).

For the following reasons we believe that the differences observed between the acoustic response of Whin Sill dolerite undergoing stress corrosion in air and in liquid water are

related to fundamental changes in crack propagation mechanism and are not due to attenuation at the boundary between specimen and medium. In experiments where we pulsed acoustic square waves of controlled characteristics through one end of a specimen and then monitored acoustic emission at the other end, the influence of attenuation at the rock/water interface was to displace amplitude distributions by -7 dB compared to tests in air, but the b-value did not change. At high values of K_I, where we believe that the same crack growth mechanism operates in wet and 'dry' tests independent of environment, b-values are much the same (Fig. 10) and amplitude distributions are displaced by approximately -7 dB. At lower K_I values, however, the b-values are considerably different between wet and 'dry' tests (Fig. 10) and amplitude distributions are displaced by -15 to -20 dB, which is more than twice that found in pulsing experiments where the only change made was in the nature of the medium surrounding the test specimen. Such a large shift in amplitude distributions cannot be entirely accounted for by attenuation at the water/rock interface, but is consistent with the idea of a change in mechanism of crack growth.

The precise nature of the change in mechanism between wet and 'dry' experiments remains unclear, but we believe that in general terms it can be explained. Atkinson & Rawlings (1981) have shown that for plagioclase feldspar in wet Black gabbro transgranular fractures occur preferentially along alteration bands of sericite particles. In air, transgranular fracture of feldspar occurs on cleavage planes inclined to these alteration bands. This phenomenon was not observed in dolerite but rather more intergranular cracking was evident for those specimens deformed wet than for those fractured in air (Figs. 15 and 16). This also seems to hold for Black gabbro and Westerly granite (Atkinson & Rawlings 1981). Increments of intergranular cracks are likely to be associated with AE events of smaller amplitude and, hence, produce an amplitude distribution characterized by a higher b-value than increments of transgranular cracks. This is because the increments in crack length around grain boundaries are likely to occur by a series of small jumps because of the small spacing between grain boundary defects. Intergranular cracking was shown earlier in this paper to be easier at lower crack velocities (lower K_I) and, hence, the pattern of b-value changes with increasing K_I (Figs 10 and 11) can readily be explained. The detailed mineralogy of the crack paths, however, will control the AE event amplitude distributions that are actually observed.

The acoustic emission results of this study taken with those of Atkinson & Rawlings (1981) argue strongly that the detailed mechanism of crack growth is strongly dependent upon crack tip environment and that the acoustic response can be used to monitor the 'humidity' of this environment and the approach of a crack to catastrophic propagation expressed in term of crack velocity and stress intensity factor. We draw attention, particularly, to the variation in the amplitude distribution parameter, b, with K_I (Figs 10 and 11). The trends shown for wet and 'dry' rocks seem virtually independent of rock type. If acoustic emission can be used as an analogue of seismicity then, in principle, changes in amplitude distribution of seismic events and seismicity rates could be used to monitor stress corrosion in the Earth. Some of the problems associated with such a study are discussed by Atkinson & Rawlings (1981). An appropriate pilot experiment might involve the study of nanoseisms (magnitude of -1 and below) recorded by borehole instruments located in known seismically active regions within a very few kilometres of the earthquake source, such as the study described by Teng & Henyey (1981).

Acknowledgments

This study was supported by grants from the Natural Environment Research Council, Nos GR3/3716 and GR3/4362. Additional support was provided by the US Geological

Survey under Contract No. 14-08-0001-18325 as part of the US National Earthquake Hazards Reduction Program. Sarah Dennis provided the details of the Preshal More basalt and Peter Swanson of CIRES, University of Colorado/NOAA, kindly furnished the specimen of Ralston Intrusive.

References

Atkinson, B. K., 1979a. Fracture toughness of Tennessee sandstone and Carrara marble using the double torsion testing method, *Int. J. Rock Mech. Min. Sci. Geomech. Abstr.*, **16**, 49–53.

Atkinson, B. K., 1979b. A fracture mechanics study of subcritical tensile cracking of quartz in wet environments, *Pure appl. Geophys.*, **117**, 1011–1024.

Atkinson, B. K., 1980. Stress corrosion and the rate-dependent tensile failure of a fine-grained quartz rock, *Tectonophys.*, **65**, 281–290.

Atkinson, B. K., 1982. Subcritical crack propagation in rock: theory, experimental results and applications, *J. struct. Geol.*, **4**, 41–56.

Atkinson, B. K., 1983. Subcritical crack growth in geological materials, *J. geophys. Res.*, in press.

Atkinson, B. K. & Meredith, P. G., 1981. Stress corrosion cracking of quartz: a note on the influence of chemical environment, *Tectonophys.*, 77, T1–T11.

Atkinson, B. K. & Rawlings, R. D., 1981. Acoustic emission during stress corrosion cracking in rocks, in *Earthquake Prediction – an International Review*, pp. 605–616, Maurice Ewing Series 4, American Geophysical Union.

Charles, R. J., 1958. Dynamic fatigue of glass, *J. appl. Phys.*, **29**, 1657–1662.

Cox, S. J. D. & Atkinson, B. K., 1982. Fracture mechanics and acoustic emission of anti-plane shear cracks in rocks, *Earthq. Predict. Res.*, **1**, 171–193.

Crampin, S., Evans, R. & Atkinson, B. K., 1984. Earthquake prediction: a new physical basis, *Geophys. J. R. astr. Soc.*, **76**, in press.

Das, S. & Scholz, C. H., 1981. Theory of time-dependent rupture in the Earth, *J. geophys. Res.*, **86**, 6039–6051.

Davidge, R. W., 1974. Effects of microstructure on the mechanical properties of ceramics, in *Fracture Mechanics of Ceramics*, Vol. 4, pp. 447–468, eds Bradt, R. C., Hasselman, D. P. H. & Lange, F. F., Plenum Press, New York.

Dilipkumar, D., Gudimetla, V. S. R. & Wood, W. E., 1979. Amplitude distribution analysis of acoustic emission, *Expl Mech.*, **19**, 438–443.

Evans, A. G., 1972. A method for evaluating the time-dependent failure characteristics of brittle materials – and its application to polycrystalline alumina, *J. Materials Sci.*, **7**, 1137–1146.

Evans, A. G. & Linzer, M., 1973. Failure prediction in structural ceramics using acoustic emission, *J. Am. Ceram. Soc.*, **56**, 575–581.

Evans, A. G., Linzer, M. & Russell, L. R., 1974. Acoustic emission and crack propagation in polycrystalline alumina, *Mater. Sci. Engrg*, **15**, 253–261.

Fuller, E. R. (Jr), 1979. An evaluation of double torsion testing – analysis, *Fracture Mechanics Applied to Brittle Materials, ASTM STP* **678**, 3–18, ed. Freiman, S. W., American Society for Testing and Materials.

Harrison, R. K., 1968. Petrology of the Little and Great Whin Sills in Woodland borehole, Co. Durham, *Bull. geol. Surv. Gt Br.*, **28**, 38–54.

Irwin, G. R., 1958. Fracture, in *Handb. Phys.*, **6**, 551–590, ed. Flügge, S., Springer-Verlag, Berlin.

Lawn, B. R. & Wilshaw, T. R., 1975. *Fracture of Brittle Solids*, Cambridge University Press, 204 pp.

Meredith, P. G. & Atkinson, B. K., 1982. High-temperature tensile crack propagation in quartz: experimental results and application to time-dependent earthquake rupture, *Earthq. Predic. Res.*, **1**, in press.

Meredith, P. G., Atkinson, B. K. & Hillman, N. B., 1981. K_{Ic} measurements on rock using a short-rod apparatus, in *Process in Experimental Petrology*, **5**, 297–298, NERC Publications Series D, No. 18.

Parsons, B. & Sclater, J. G., 1977. An analysis of the variation of ocean floor bathymetry and heat flow with age, *J. geophys. Res.*, **82**, 803–827.

Pollock, A. A., 1973. Acoustic emission – 2: acoustic emission amplitudes, *Non-Destruct. test.*, **6**, 264–269.

Pollock, A. A., 1974. Acoustic emission: a review of recent progress and technical aspects, in *Acoustics and Vibration Progress*, **1**, 53–84, eds Stephens, R. W. B. & Leventhal, H. G., Chapman & Hall, London.

Pollock, A. A., 1980. Acoustic emission amplitude distributions, in *International Advances in Nondestructive Testing,* **7**, ed. McGonnagle, W. J., in press.

Sano. O. & Ogino, S., 1980. Acoustic emission during slow crack growth, *Tech. Rep. Yamaguchi Univ.,* **2**, 381–388.

Swanson, P. L., 1980. Stress corrosion cracking in Westerly granite: an examination by the double torsion technique, *MSc thesis,* University of Colorado.

Swanson, P. L., 1983. Subcritical crack growth and other time and environment dependent behaviour in crustal rocks, *J. geophys. Res.,* in press.

Teng. T. & Henyey, T. L., 1981. The detection of nanoearthquakes, in *Earthquake Prediction – an International Review,* pp. 533–542, Maurice Ewing Series 4, American Geophysical Union.

Trantina, G. G., 1977. Stress analysis of the double torsion specimen, *J. Am. Ceram. Soc.,* **60**, 338–341.

Van Horn, R., 1976. Geology of the Golden Quadrange, Colorado, *Prof. Pap. U.S. geol. Surv. 872.*

Wadley, H. N. G., Scruby, C. B. & Shrimpton, G., 1981. Quantitative acoustic emission source characterization during low temperature cleavage and intergrannular fracture, *Acta metall.,* **29**, 399–414.

Waza, T., Kurita, K. & Mizutani, H., 1980. The effect of water on the subcritical crack growth in silicate rocks, *Tectonophys.,* **67**, 25–34.

Wiederhorn, S. M., 1974. Subcritical crack growth in ceramics, in *Fracture Mechanics of Ceramics,* **2**, 613–646, eds Bradt, R. C., Hasselman, D. P. H. & Lange, F. F., Plenum Press, New York.

Wiederhorn, S. M., 1978. Mechanisms of subcritical crack growth in glass, in *Fracture Mechanics of Ceramics,* **4**, 549–580, eds Bradt, R. C., Hasselman, D. P. H. & Lange, F. F., Plenum Press, New York.

Wilkins, B. J. S., 1980. Slow crack growth and delayed failure of granite, *Int. J. Rock Mech. Min. Sci. Geomech. Abstr.,* **17**, 365–369.

Williams, D. P. & Evans, A. G., 1973. A simple method for studying slow crack growth, *J. test. Eval.,* **1**, 264–270.